Experimental analysis of late direct injection combustion mode in a compression-ignition engine fuelled with biodiesel/diesel blends

José Antonio Vélez Godiño [A] (corresponding author), Miguel Torres García [B], Francisco José Jiménez-Espadafor Aguilar [B],

[A] Departamento de Máquinas y Motores Térmicos, Universidad de Cádiz. Escuela Superior de Ingeniería, Avda. Universidad de Cádiz, nº 10, 11519, Puerto Real (Cádiz), Spain.

[B] Departamento de Ingeniería Energética, Universidad de Sevilla. Escuela Técnica Superior de Ingeniería de Sevilla, Camino de los Descubrimientos, s/n, 41092, Seville, Spain.

Highlights

Modified diesel engine with late direct injection and rapeseed biodiesel.

Biodiesel combustion analysis allows characterization of engine performance.

NOx emissions are significantly reduced compared to conventional diesel combustion.

Accurate models of autoignition delay and combustion duration are proposed.

Abstract

A compression ignition reciprocating internal combustion engine has been modified to allow operation with late direct injection of rapeseed biodiesel fuel blends. The purpose of these modifications is to reduce both the engine's carbon footprint and emission of nitrogen oxides and soot, without decreasing performance or using expensive emission post-treatment systems. The experimental part of this work is based on the measurement of the main pollutants being emitted and the analysis of the combustion process, which is accomplished by the study of the heat release rate curve. This curve is derived from the experimental chamber pressure data, in combination with a zero-dimensional thermodynamic model assuming a perfect mixing reactor with temporal variation in volume and chemical composition, temperature-dependent properties and heat losses. The analysis of the experimental results allows deepening the knowledge of the combustion process in a compression ignition engine with late direct injection using different biodiesel blends. There is a significant reduction (> 50%) of emissions of nitrogen oxides in comparison with the original configuration. This allows considering the modified configuration as an advanced combustion mode, intermediate between conventional compression ignition engines and homogeneous charge compression ignition combustion mode.

Keywords

Compression ignition engine

Late injection

Biodiesel

Exhaust Gas Recirculation (EGR)

Emissions

Heat Release Rate (HRR)

Nomenclature

ABDC After bottom dead center

ATDC After top dead center

B Bore

BMEP Brake mean effective pressure

BSU Bosh smoke units

BTDC Before top dead center

CAD Crank angle degree

CFD Computational fluid dynamics

CI Compression ignition

CO Carbon monoxide

CO_2 Carbon dioxide

Cp Specific heat capacity

Cm Mean piston speed

EA Energy of activation

EGR Exhaust gas recirculation

EOC End of combustion

EVC Exhaust valve close

EVO Exhaust valve open

F Fuel/air equivalence ratio

FAME Fatty acid methyl ester

h Instantaneous heat transfer coefficient

HC Hydrocarbons

HCCI Homogeneous charge compression ignition

HRR Heat release rate

IVC Inlet valve close

IVO Inlet valve open

LHC Lower heating value

NOx Nitrogen oxides

p Pressure

Q Heat

R Ideal gas constant

rpm Revolutions per minute

SOC Start of combustion

SOI Start of injection

t Time

T Temperature

v Volume

v_s Tangential speed

x_B Fuel mass fraction burned

γ Specific heat ratio

θ Crank angle

τ Combustion delay

ω Angular speed

1. Introduction

Biodiesel is a fuel composed of fatty acid methyl esters (FAME) derived from transesterification with methanol of fats of typically vegetable origin [1]. The main advantage of the use of biodiesel as a fuel in reciprocating internal combustion engines lies in its renewable origin, which is why its combustion is considered neutral in carbon dioxide (CO_2) emissions, due to the assimilation process encompassed in the photosynthesis carried out by the plant. Furthermore, the use of biodiesel as a fuel in compression ignition (CI) engines reduces the levels of emissions of carbon monoxide (CO), soot and unburnt hydrocarbons (HC) [2]. Other advantages associated with the use of biodiesel consist of a higher cetane number than that corresponding to fossil diesel fuel and a very low content of sulphur and aromatic compounds [3]. However, the use of biodiesel in reciprocating internal combustion engines entails a series of drawbacks, such as a lower energy density than fossil diesel fuel, as well as higher

viscosity values, cloud point and pour point [4]. Furthermore, another drawback of the use of biodiesel in internal combustion engines is the slight increase in emissions of nitrogen oxides (NOx) compared to fossil diesel fuel [5]. Among the reasons for this slight increase in NOx emissions, it is worth highlighting [6]:

- The kinetic mechanisms of biodiesel oxidation are different from those of fossil diesel fuel.
- The higher cetane number in biodiesel implies the advancement of combustion, which increases the maximum temperature reached in the chamber.
- The adiabatic flame temperature of oxygenated fuels, such as biodiesel, is higher than that of fossil diesel fuel.
- The lower soot emissions associated with the combustion of biodiesel implies a lower radiative heat loss, which increases the temperature of the gases.
- The different properties of biodiesel regarding the mixture formation influence the portion of energy released in the premixed and diffusive combustion phases.

Within the framework of CI engines there are several advanced modes of combustion (e.g.: homogeneous charge compression ignition, partially premixed compression ignition, reactivity controlled compression ignition, ...), which have as their main task to improve the performance of the combustion, either in terms of power and/or of emission of pollutants [7]. Among the mentioned advanced modes of combustion is late direct injection. The term “late” is due to the fact that the fuel injection occurs later than in a conventional diesel engine. However, this delay in the fuel injection is shorter than that used in the system known as Modulated Kinetics (MK) [8] [9] [10]. The main attraction of the use of late direct injection is its potential to reduce NOx emissions, due to the decrease in average temperature during the combustion stage [11], as detailed in Section 2. However, this also leads to one of the main drawbacks of this combustion mode: the decrease in NOx emissions is accompanied by an increase in soot emissions.

The achievement of the ultra-low levels of NOx and soot emissions imposed by the legislation in force constitutes one of the main determining factors in the design of future reciprocating internal combustion engines [12] [13]. The objective of this work is to evaluate the possibility of reducing NOx emissions without the need to employ expensive emission post-treatment systems, while avoiding compromising the typical levels of the engine’s thermal efficiency. To achieve this objective, the use of fossil diesel fuel mixtures with biodiesel is proposed, in different percentages, in combination with a late direct injection system. In this way, the increase in soot emission levels derived from this injection system will be offset by the reduction derived from the use of biodiesel as fuel. Likewise, the slight increase in NOx emissions derived from the oxidation of biodiesel will be offset by the reduction associated with the late direct injection strategy. To achieve this objective, in addition to considering the emission of the main pollutants, special attention will be paid to the study of both the ignition delay and the combustion duration, which will be done through the study of the heat release rate (HRR). From this analysis, the possibility of establishing suitably validated functional laws for the ignition delay and the combustion duration will be evaluated, which in the future will constitute the foundation of a predictive model of this mode of combustion.

The present work is divided into three main blocks. First, the details corresponding to the test bench designed to obtain the experimental data will be presented, including the characteristics of the studied engine, the instrumentation and the different fuels used. Next, the main characteristics of the mathematical model used for the combustion analysis will be exposited, which will make it possible to obtain the

HRR curves. Subsequently, the results obtained in relation to both the pollutant emissions and the ignition delay and the combustion duration will be analysed. Finally, the main conclusions derived from the experimental analysis developed will be presented.

2. Experimental setup

The experimental data analysed in this work have been obtained from a single cylinder four-stroke engine, compression ignition, direct injection, naturally aspirated and air-cooled, model Deutz FL1 906 (Fig. 1, left). Although originally the engine would develop a rated power of 11 kW at 3000 rpm and a maximum torque of 45 Nm at 2100 rpm, a series of modifications have been carried out to optimize its operation with late direct injection, whose start of injection (SOI) is set 10 CAD BTDC. The characteristics of the analysed engine after making the modifications are listed in Table 1.

Table 1: Specifications of the modified Deutz FL1 906 engine.

Parameter	Value
Displacement	708 cm^3
Bore	95 mm
Stroke	100 mm
Compression ratio	18.4:1
Piston bowl diameter	34.5 mm
Injection pump	Mechanical
Nozzle opening pressure	300 bar
No. injection holes	5
Injection hole diameter	0.26 mm
IVO / IVC	-2 / 36 CAD ATDC
Inlet valve diameter	44 mm
EVO / EVC	-36 / 2 CAD ABDC
Exhaust valve diameter	38 mm
Maximum valve lift	12 mm
Lube oil system	Gear pump
Cooling system	Fan by flywheel

To reduce NOx emissions, it is necessary to enhance both the evaporation of the fuel and its subsequent mixing with the air, so that at the onset of combustion there is a composition in the chamber that is as homogeneous as possible. Since the conditions in the chamber during late direct injection imply a minimization of the autoignition delay due to the proximity of the TDC, measures are required to avoid the combustion of a heterogeneous charge. This is due to the fact that the temperature levels during late direct injection allow a vertiginous increase in the concentration of radicals that promote the appearance of H_2O_2, whose presence is considered the trigger for combustion ignition [14] [15]. Possible measures to increase delay in late direct injection engines include cooled exhaust gas recirculation (EGR), a tool commonly used in diesel engines to reduce NOx emissions. The use of EGR is based in the introduction of a fraction of the exhaust gases in the engine cylinder, causing a decrease in the temperatures during combustion [16]. Likewise, to promote the evaporation of the fuel and its mixture with the air, it is possible to increase the level of turbulence in the combustion chamber. To do this, maximizing the initial turbulence through external mechanisms (initial swirl) is ruled out, since this would imply greater heterogeneity in the temperature field due to increased heat losses, finally resulting in higher levels of pollutant emissions and, even, in lower efficiency [17]. On the contrary, the use of internal induction mechanisms is

considered adequate, which maximize the level of turbulence when the piston is close to the TDC (internal swirl). Among these mechanisms, the adoption of high-swirl chamber pistons, instead of the traditional disc pistons, stands out. Although the original engine already had a bowl-in-piston combustion chamber, it was found that the induced turbulence levels were insufficient and therefore the diameter of the piston bowl had to be reduced. For this reason, the original piston, with a ratio between cylinder and chamber diameter of 1.6, was replaced by another design with a greater capacity to induce swirl, with a ratio of 2.8. In this way, by combining the cooled EGR and the internal turbulence induction mechanisms, it is intended to achieve a delay in the start of combustion and a reduction of the maximum value of the HRR curve, which will ultimately lead to lower levels of NOx formation.

In addition to the change in the start of injection angle, to improve the conditions in the tests in which biodiesel is used as fuel, the fuel injection system was modified to increase the maximum injection pressure from its original 450 bar to a value of 650 bar. This is intended to contribute to improving the homogeneity of the mixture, reducing the injection time and increasing the surface-volume ratio of the injected fuel droplets, which contributes to a faster evaporation of the fuel.

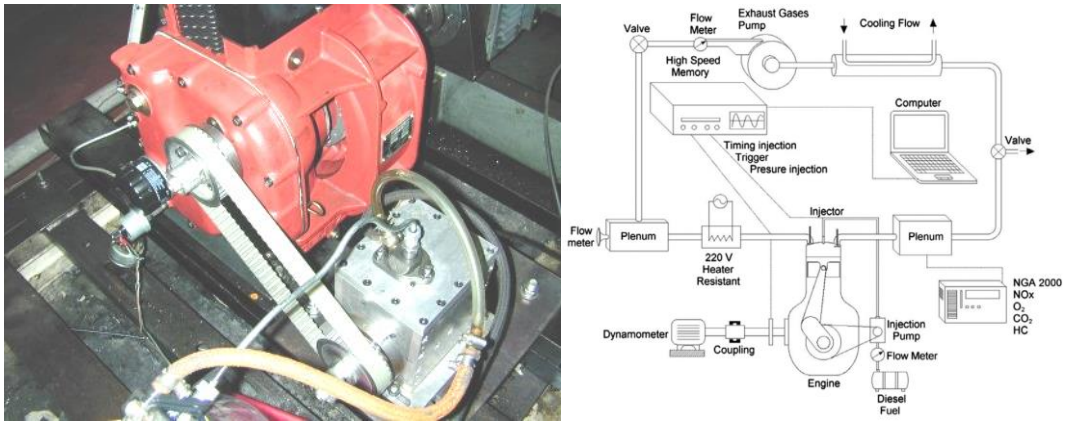

Fig. 1: Analysed engine (Deutz FL1 906 model) and test bench scheme.

A diagram of the designed test bench is shown in Fig. 1 (right). In addition to the previously mentioned modifications in relation to the cooled EGR and the fuel injection systems, this figure shows the installation of a stagnation box in the intake and an expansion tank in the exhaust, in order to eliminate the strong pulsating waves generated by the operation of the single-cylinder engine. As can be seen in Fig. 1 (right), control of the torque and the rotation speed is carried out by means of a 25 kW electric dynamometric brake, with a variable frequency drive and a load cell to measure the generated torque.

In addition to the previously mentioned systems, the test bench is equipped with the following monitoring instrumentation:

- High frequency data acquisition system, Iotech DAQ 3000 (16 bit, 1 MHz).
- Crankshaft angle encoder, Kistler 2613B, with an accuracy of 0.02 CAD.
- The absolute pressure in the combustion chamber is obtained from a combination of the signals from a water-cooled piezoelectric sensor, Kistler 6061B, and the intake pressure measured by a piezo-resistive probe, Kistler 4045A10.
- Exhaust gas analyser, Fisher-Rosemount NGA 2000, whose main characteristics are shown in Table 2.

Table 2: Exhaust gas analyser specifications.

Parameter	Sensor	Range	Accuracy
O_2	Paramagnetic	0 - 5%vol	± 0.04%vol
		0 - 100%vol	± 0.8%vol
CO	Non-dispersive infrared	0 - 5,000 ppm	± 5.0 ppm
		0 - 100,000 ppm	± 5,000 ppm
CO_2	Non-dispersive infrared	0 - 20%vol	± 1%vol
NOx	Chemiluminescence	0 - 250 ppm	± 12.5 ppm
		0 - 1,000 ppm	± 50 ppm
		0 - 2,500	± 125 ppm
		0 - 10,000	± 1,000 ppm
HC	Flame ionization	0 - 1,000 ppm	± 50 ppm
		0 - 20,000 ppm	± 1,000 ppm

To carry out the experimental tests included in the present analysis, both diesel fuel of fossil origin (EN-590), hereinafter B0, and mixtures of it with rapeseed biodiesel (EN-14214) at 30% and 65%, hereinafter B30 and B65 respectively, were used. Table 3 shows the main properties of the tested fuels, which were laboratory characterized. Analysing Table 3 it can be concluded that the incorporation of biodiesel into the fuel leads to a notable increase in viscosity and density, as well as a displacement of the distillation curve towards the higher temperature range. These characteristics, together with the higher surface tension of biodiesel, result in a larger droplet size, greater penetration of the injected fuel spray and greater difficulty in evaporating it. This increases the risk of the fuel being deposited in a liquid state on the chamber walls, which would lead to a loss of efficiency, higher emissions of carbon monoxide and unburnt hydrocarbons, and even the possibility of causing mechanical damage to the cylinder due to the destruction of the lube oil film.

Table 3: Main properties of the tested fuels.

Property	B0	B30	B65	B100
Density, at 15ºC (kg/m3)	832.0	858.8	865.5	883.4
Viscosity, at 40ºC (cSt)	2.9	3.3	4.0	4.6
LHV (MJ/kg)	43.1	42.2	41.2	40.2
95% distillation temperature	175-350	200-390	207-405	320-415
Cetane index	47.0	47.6	52.2	52.6
Reduced formula	$CH_{1.9}$	-	-	$CH_{1.85}O_{0.11}$
Stoichiometric A/F	14.7	-	-	13.0

For each fuel mixture considered, different conditions of speed, load and percentage of external EGR were analysed. The control strategy of the EGR system is “constant fuelling rate” to that of the no EGR case. This approach leads to different fuel-to-air ratios increasing with the EGR rate. Since the injected fuel is constant, the power output is almost equal (slight drop), hence making the comparison fair and logical [18]. The ranges of variation of each of these four operating variables are defined in Table 4. In the case of the percentage of external EGR, the analysed range extends from null values to the value that implied, for each combination of fuel blend, speed and load, an erratic engine operation (due to misfire), having reached a maximum value of 41%. The tests carried out show that the higher the engine load, the lower the maximum percentage of EGR, due to the higher concentration of combustion products.

Table 4: Operating conditions involved in the experimental tests.

Variable	Values
Fuel	B0, B30, B65
Speed (rpm)	1800, 2100, 2400
Fuel/air equivalence ratio	0.20, 0.30, 0.45, 0.60
EGR (%)	From 0 to 41

3. Modelling

Given that the objective of this work is to analyse the combustion derived from the use of a late direct injection, it is essential to have a model that allows obtaining the HRR from the chamber pressure data corresponding to the tests carried out, both with fossil diesel fuel and with mixtures with different percentages of rapeseed biodiesel. For this reason, a zero-dimensional thermodynamic model has been used, through which the combustion chamber is considered to be a perfect mixing reactor, with temporal variation in volume and chemical composition, temperature-dependent properties and heat losses through the chamber walls [19] [20].

By combining the first principle of thermodynamics and the state equation of ideal gases, the expression that allows characterizing the HRR can be obtained from the chamber pressure curve [21]:

$$HRR = \frac{dQ_{fuel}}{d\theta} = \frac{1}{\gamma-1}\left(p \cdot \gamma \cdot \frac{dv}{d\theta} + v \cdot \frac{dp}{d\theta}\right) - \frac{p \cdot v}{(\gamma-1)^2} \cdot \frac{d\gamma}{d\theta} - \frac{dQ_{HL}}{d\theta} \qquad \text{Eq. 1}$$

The last term of the right-hand side of Eq. 1 ($^{dQ_{HL}}/_{d\theta}$) represents the heat losses through the combustion chamber walls. Also, as can be seen in Eq. 1, the model considers the sensible heat corresponding to the injected fuel to be negligible, although it does consider the effect of the variation of the properties with temperature and chemical composition.

The effect of temperature on the thermodynamic properties of the main chemical species present in the mixture has been modelled by polynomial functions (Eq. 2) whose coefficients have been obtained from the NASA JANAF thermodynamic data tables [22]:

$$\frac{C_P}{R} = a_1 + a_2 \cdot T + a_3 \cdot T^2 + a_4 \cdot T^3 + a_5 \cdot T^4 \qquad \text{Eq. 2}$$

The heat losses through the combustion chamber walls have been modelled using the instantaneous cylinder average heat transfer coefficient h_g (Eq. 3) proposed by Woschni [23] for direct injection IC engines:

$$h_g = 3.26 \cdot \frac{p^{0.8}}{B^{0.2} \cdot T^{0.55}} \cdot \left[C_1 \cdot c_m + C_2 \cdot \frac{V_d \cdot T_{ivc}}{p_{ivc} \cdot v_{ivc}} \cdot (p - p_m)\right]^{0.8} \qquad \text{Eq. 3}$$

Different variables are involved, such as the combustion chamber pressure p and temperature T, the cylinder bore B, the mean linear piston speed c_m, the engine displacement V_d, the temperature, the pressure and the volume of the chamber at a reference point, considered as the ivc and, finally, the pressure in the chamber in the absence of combustion p_m. The term in brackets in Eq. 3 represents the characteristic speed of the gas inside the combustion chamber, which considers the contribution derived from both the movement of the piston and the change in density experienced during combustion. The values corresponding to C_1 and C_2 are shown in Table 5.

Table 5: Values C_1 and C_2 used in the Woschni correlation (Eq. 3).

Stroke	C_1	C_2
Compression	$2.28 + 0.308 \cdot \frac{v_s}{c_m}$	0
Combustion y expansion	$2.28 + 0.308 \cdot \frac{v_s}{c_m}$	$3.24 \cdot 10^{-3}$

Here, v_s is the tangential speed derived from the swirl, which has been accounted for from a previously experimentally validated model [24]. In this way, the model used for the present combustion analysis takes into account the effect on heat losses derived from the adoption of internal turbulence induction mechanisms.

Finally, it should be noted that, for each test considered, the chamber pressure curve used in the analysis results from averaging 150 consecutive cycles (COV_{IMEP}<5%) [19] [25].

4. Results

4.1. Analysis of performance and pollutant emissions

The experimental tests carried out have made it possible to characterize the performance of the analysed engine working with different percentages of biodiesel after being modified to operate with late direct injection. Firstly, a comparison between the most characteristic results of the original and the modified configurations is shown in Fig. 2. The modifications related to the adoption of the late direct injection strategy have not led to a relevant reduction in engine performance in terms of BMEP, since the maximum values of this parameter experienced a decrease of only 6.9% compared to the original configuration (Fig. 2, left). This shortfall is acceptable based on the significant reduction of NOx emissions shown in Fig. 2 (right) for the modified configuration, where the NOx decrease at high loads is higher than 50% compared to the original configuration.

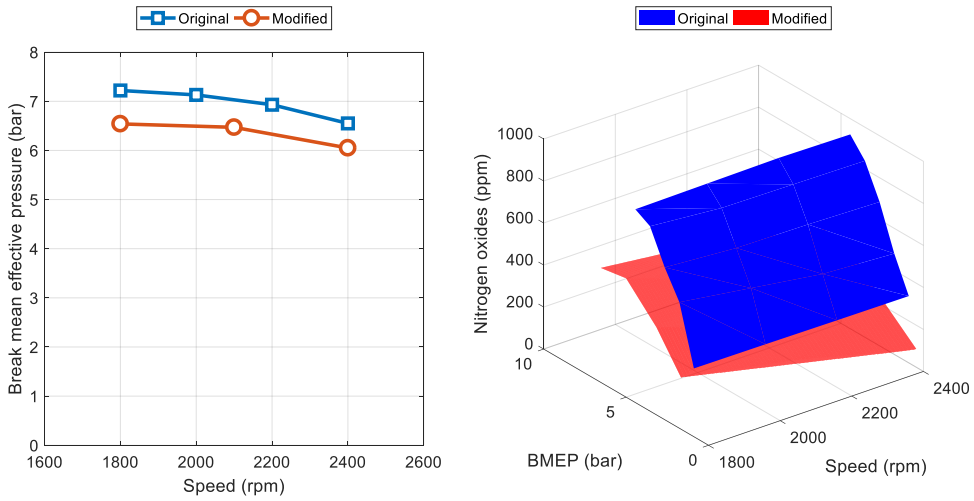

Fig. 2: Comparison between the original and the modified engine configurations (left: maximum BMEP, right: NOx emissions without external EGR).

Among the results obtained is the brake efficiency, showing in Fig. 3 the performance maps corresponding to each of the three fuel mixtures used for tests without external EGR. It can be observed that the maximum efficiency experiences an increase

as the percentage of biodiesel increases. This increase in brake efficiency is attributed to the higher cetane index of biodiesel compared to fossil diesel fuel, which reduces the delay in the start of combustion for higher percentages of biodiesel, increasing the expansion work, as will be seen in more detail later.

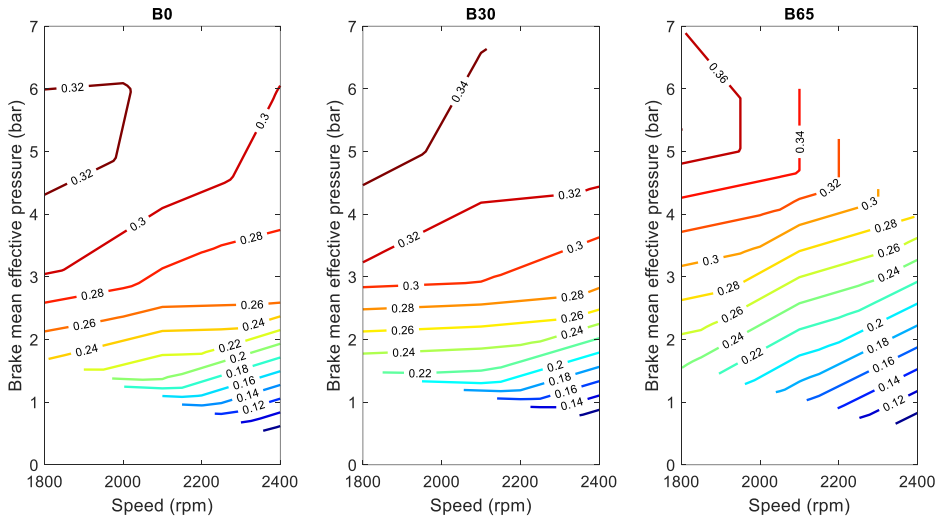

Fig. 3: Brake efficiency (dimensionless) maps (left: B0, middle: B30, right: B65) corresponding to 0% external EGR.

By combining the chamber pressure curves obtained from the experimental tests and the thermodynamic model described in Section 3, the temporal evolution of both the HRR and the fuel mass fraction burned (X_B) can be obtained. In the case of the HHR, throughout this work its normalized values ($HRR = {dX_B}/{d\theta}$) will be shown, in order to cancel the effect of the different LHV of the different fuel mixtures used, this being greater for the fossil diesel fuel than for the rapeseed biodiesel (see Table 3). An example of the results obtained by applying this method is illustrated in Fig. 4. The start of combustion (SOC) has been established for $X_B^{SOC} = 5\%$, a common practice in the study of the development of combustion due to the uncertainty associated with the identification of the SOC as a consequence of the high noise level in the chamber pressure experimental signal [26] [27] [28]. Likewise, the end of combustion (EOC) has been established for $X_B^{EOC} = 95\%$, thus disregarding the end of combustion, during which it develops very slowly and whose analysis does not provide relevant information to the study [29]. In relation to Fig. 4 it should also be noted that, as derived from the HRR and X_B curves, the development of combustion derived from the use of late direct injection in the analysed engine results in a combustion composed of two phases, premixed and diffusive. This makes it possible to conclude that the mixture achieved inside the cylinder is not completely homogeneous, despite the fact that, according to the injection system data, the injection has ended at the start of combustion.

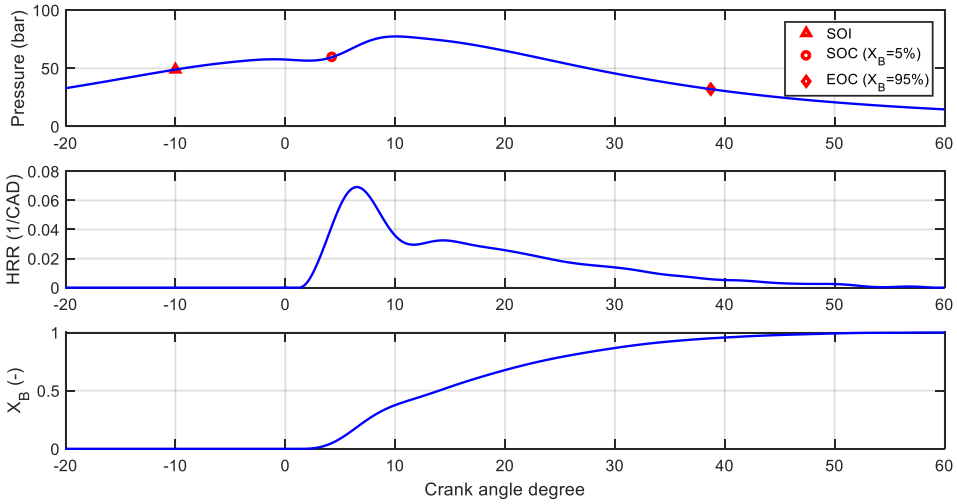

Fig. 4: Cylinder pressure (top), heat release rate (middle) and fuel mass fraction burned (bottom) corresponding to B65, 1800 rpm, 0.45 fuel/air equivalence ratio and 0% external EGR.

However, the NOx emissions data of Fig. 5 show that the measures implemented in the modified engine have made it possible to achieve a greater degree of homogeneity than in a conventional IC engine. In other words, the NOx emissions associated with the B0 fuel in the configuration modified to operate with late direct injection represent less than half of the emissions corresponding to the same fuel with the original engine [30], without reducing its performance. This allows concluding that the homogeneity of the mixture in the cylinder increases compared to the initial configuration of the engine. Likewise, this reduction in NOx emissions shows a decrease in the maximum temperatures achieved inside the combustion chamber, which implies that the effect of radiation heat transfer is less relevant, which is consistent with the heat loss model adopted (Section 3). In relation to the modified configuration, Fig. 5 also shows the previously mentioned slight increase in NOx emissions associated with the use of biodiesel, due to the effects mentioned in Section 1, among which the shorter ignition delay corresponding to biodiesel stands out, which implies higher average temperatures in the combustion chamber. To conclude the analysis of NOx emissions, Fig. 6 shows their behaviour against the percentage of external EGR and the fuel/air equivalence ratio, encompassing tests carried out at 1800 rpm for the three fuel mixtures analysed (B0, B30 and B65). This confirms, firstly, the usefulness of cooled EGR as a tool for reducing NOx emissions, despite the slight increase in specific fuel consumption associated with the longer ignition delay and, consequently, lower expansion work. Secondly, Fig. 6 shows the direct proportionality between the NOx emissions and the fuel/air ratio, due to the increase in the combustion chamber temperature derived from the oxidation of a greater quantity of fuel.

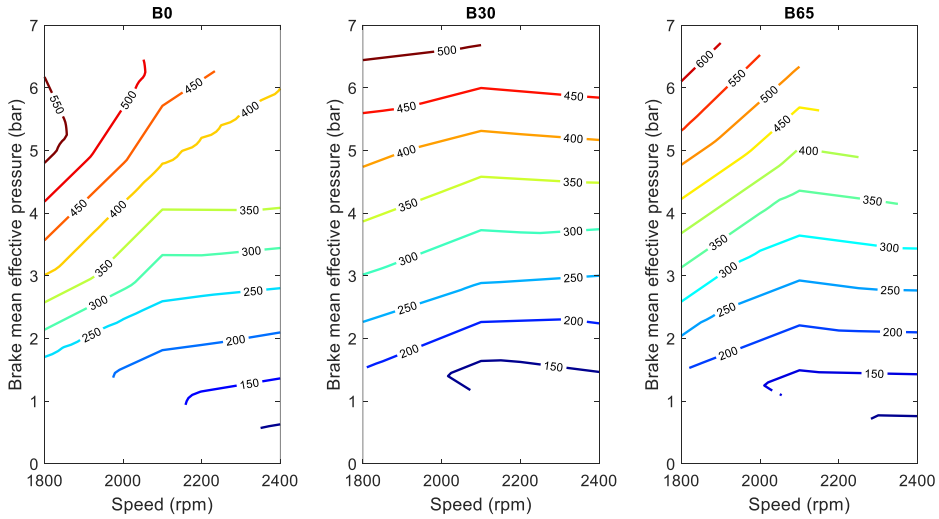

Fig. 5: NOx emissions (ppm) maps (left: B0, middle: B30, right: B65) corresponding to 0% external EGR.

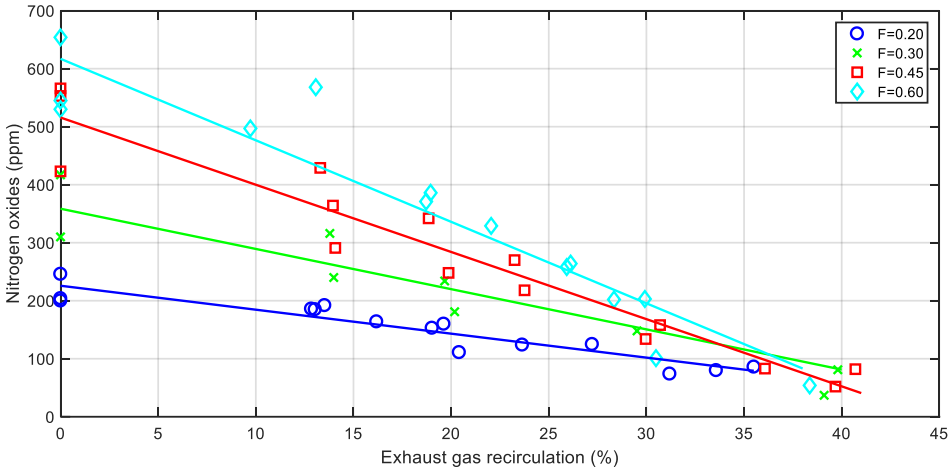

Fig. 6: NOx emissions (ppm) as a function of external EGR (%), for different fuel/air equivalence ratios at 1800 rpm, including B0, B30 and B65.

Fig. 7 shows CO emissions versus variations in external EGR and fuel composition, given fixed speed and fuel/air equivalence ratio. In this case, the increase in the amount of external EGR leads to an increase in CO emissions, which is attributed to the decrease in the average temperature of the gases in the combustion chamber. This drop in temperature is associated with both the capacitive effect of the cooled EGR and the longer delay in the SOC during the expansion stroke. Additionally, Fig. 7 allows observing the effect of the percentage of biodiesel on CO emissions. It can be concluded that a higher proportion of biodiesel results in lower CO emissions. This effect is associated with the previously mentioned increase in the average temperature of the gases during combustion due to the shorter delay in the SOC derived from biodiesel.

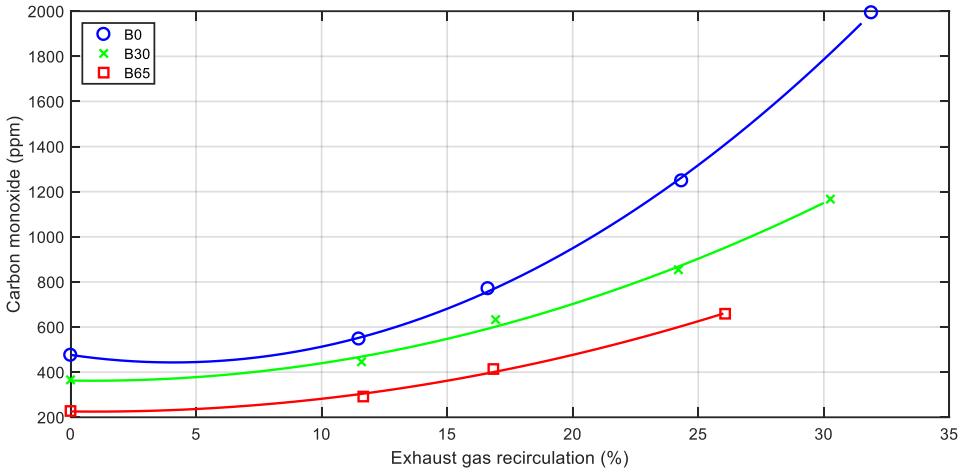

Fig. 7: CO emissions (ppm) as a function of external EGR (%), for different fuel mixtures at 1800 rpm and 0.45 fuel/air equivalence ratio.

Similarly to Fig. 7, Fig. 8 shows HC emissions versus variations in external EGR, given fixed speed and fuel/air equivalence ratio. As in Fig. 7, an increase in HC emissions derives from the increase in the amount of external EGR, which is attributed to the same reason as the CO emissions increase referred in the previous paragraph: the decrease in the average temperature of the gases in the combustion chamber, derived from both the capacitive effect of the cooled EGR and the longer delay in the SOC during the expansion stroke.

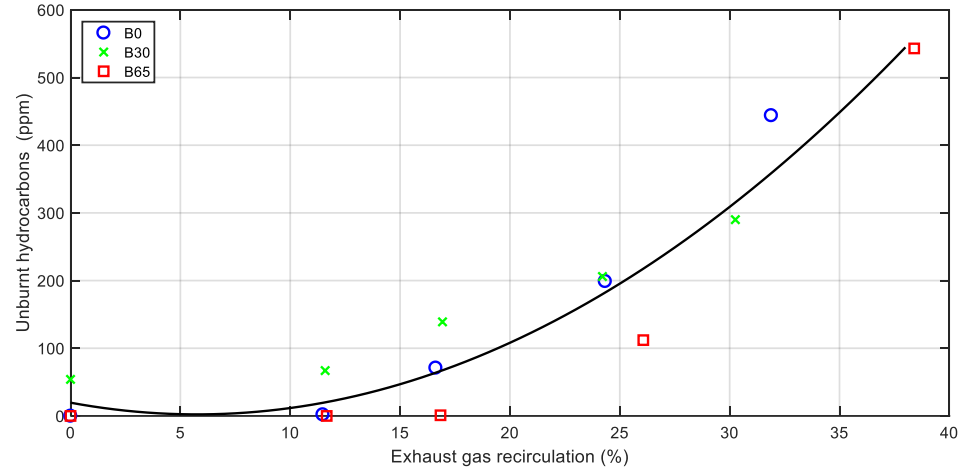

Fig. 8: HC emissions (ppm) as a function of external EGR (%), for different fuel mixtures at 2100 rpm and 0.45 fuel/air equivalence ratio.

To conclude the analysis of the emissions, the levels of soot are characterized from the smoke opacity index (Fig. 9), which ranges from 0 (white) to 10 (intense black). Although the figure shows the evolution of the smoke opacity index versus the percentage of external EGR, in Fig. 9 (A) the parameter used is the fuel composition, while in Fig. 9 (B) the parameter is the fuel/air equivalence ratio. Both Fig. 9 (A) and (B) show the increase in soot emissions derived from an increase in the percentage of external EGR, an effect widely present in conventional IC engines due to the reduction in available oxygen. However, Fig. 9 (A) evidences that an increase of biodiesel percentage in the fuel mixture results in lower soot emissions, as mentioned in Section

1. This reduction in soot emissions is associated to the lower stoichiometric oxygen needed to carry out the combustion. In addition, Fig. 9 (B) reflects the evident increase in soot emissions derived from the increase in engine load.

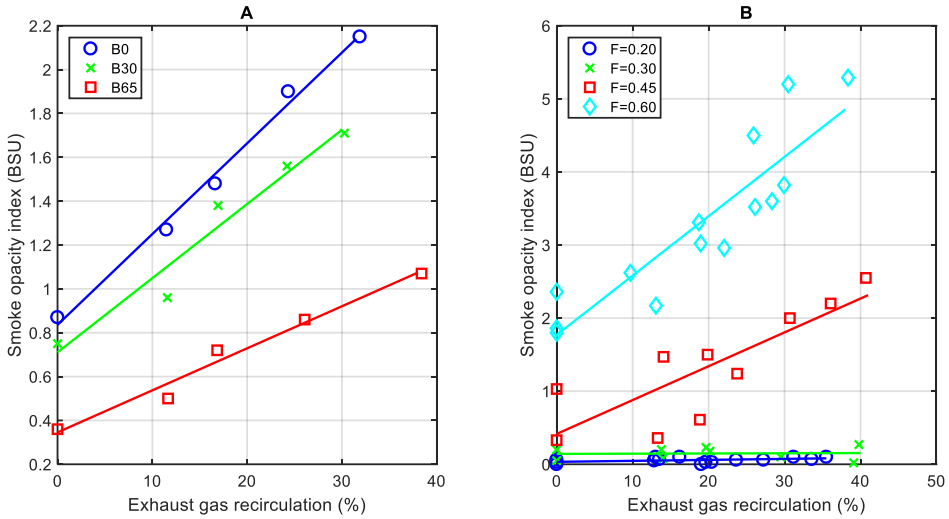

Fig. 9: Smoke opacity index (BSU) as a function of external EGR (%). A: Different fuel mixtures at 2400 rpm, 0.45 fuel/air equivalence ratio. B: Different fuel/air equivalence ratios at 1800 rpm.

4.2. Analysis of ignition delay

Regarding the analysis of the combustion process, the ignition delay has been analysed first. This delay is defined as the period (expressed in time or angle) between the start of injection (SOI) and the start of combustion (SOC), set as the point at which the fuel mass fraction burned achieves 5% (Fig. 4). In Fig. 10, the delay time is represented against the engine load, using different fuel mixtures as a parameter. It is observed that the greater the load, the shorter the delay. This effect is explained as a consequence of the heating that the engine experiences when the load increases, which finally translates into an increase in the temperature of the gas in the cylinder, which reduces the ignition delay. Furthermore, as previously mentioned, the lower cetane number of biodiesel (Table 3) implies that the higher the percentage of biodiesel in the fuel mixture, the shorter the measured delay.

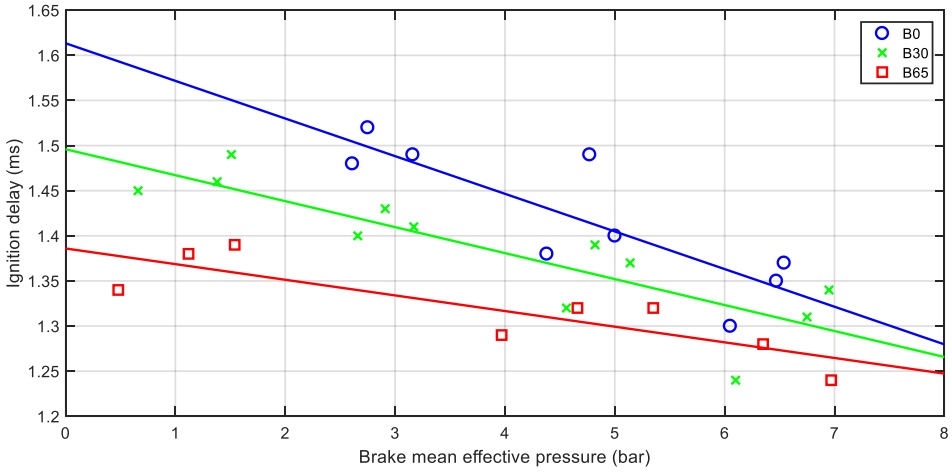

Fig. 10: Ignition delay (ms) as a function of break mean effective pressure (bar), for different fuel mixtures at 0% external EGR, including 1800, 2100 and 2400 rpm.

In Fig. 11 the delay angle versus the percentage of external EGR is shown, using the fuel composition as a parameter in Fig. 11 (A), while in Fig. 11 (B) the parameter used is the engine speed. Both figures show that there is a practically linear increase in the ignition delay derived from an increase in the percentage of external EGR, as a consequence of the increase in the heat capacity of the mixture due to the higher fraction of combustion products presented in the mixture. Furthermore, Fig. 11 (A) again shows that the higher the biodiesel fraction, the shorter the delay. In addition to the previously mentioned effect of the cetane index, the fact that the delay is shorter for biodiesel causes higher average temperatures in the combustion chamber, which enhances the advance effect caused by biodiesel. In addition, Fig. 11 (B) reflects the effect of engine speed according to which, as in conventional IC engines, the delay angle increases with speed. Although an increase in engine speed implies a decrease in delay time due to increased turbulence, the delay angle increases, since the decrease in delay time is proportionally less than the increase in engine speed ($\Delta\theta = \varpi \cdot \Delta t$) [31].

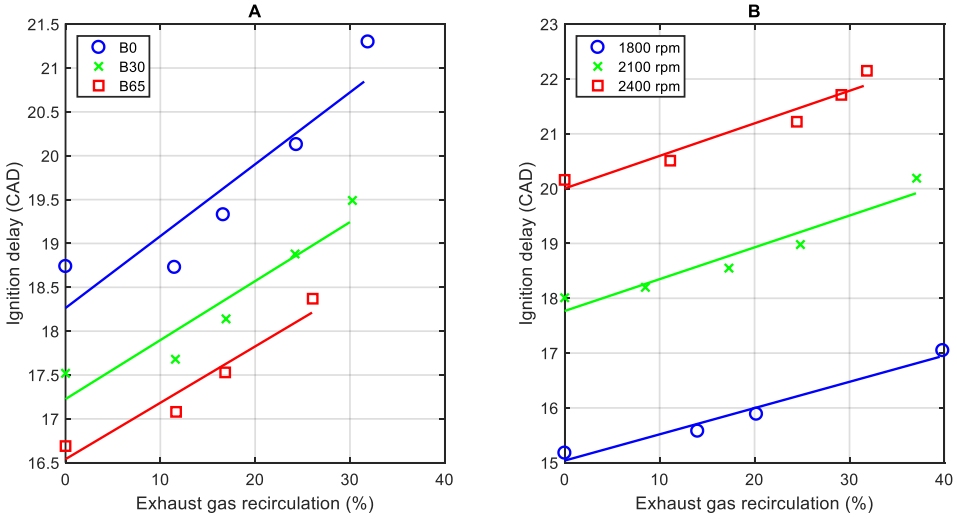

Fig. 11: Ignition delay (CAD) as a function of external EGR (%). A: Different fuel mixtures at 2100 rpm, 0.45 fuel/air equivalence ratio. B: Different engine speeds for B30 and 0.30 fuel/air equivalence ratio.

4.3. Analysis of heat release rate

The analysis of the evolution of the normalized HRR versus variations in the different operating parameters is presented now. Before proceeding to the analysis of the results shown, it should be clarified that the represented HRR curve is normalized ($HRR = {dX_B}/{d\theta}$), therefore its absolute values (J / CAD) are not shown, which would logically be higher the greater the fuel/air equivalence ratio considered. In Fig. 12 (A) the influence of the percentage of biodiesel in the fuel mixture is shown. First, it can be verified that, as previously mentioned, higher proportions of biodiesel imply an early start of combustion, as a consequence of the higher cetane number associated with biodiesel. In addition, this figure reveals that, despite presenting a shorter delay and therefore a higher temperature of the mixture at the beginning of combustion, the higher the percentage of biodiesel, the lower the maximum of the HRR curve. This trend is due to the reduction of the delay time, which implies a lower fraction of evaporated fuel and, consequently, a lower energy released during the premixed phase.

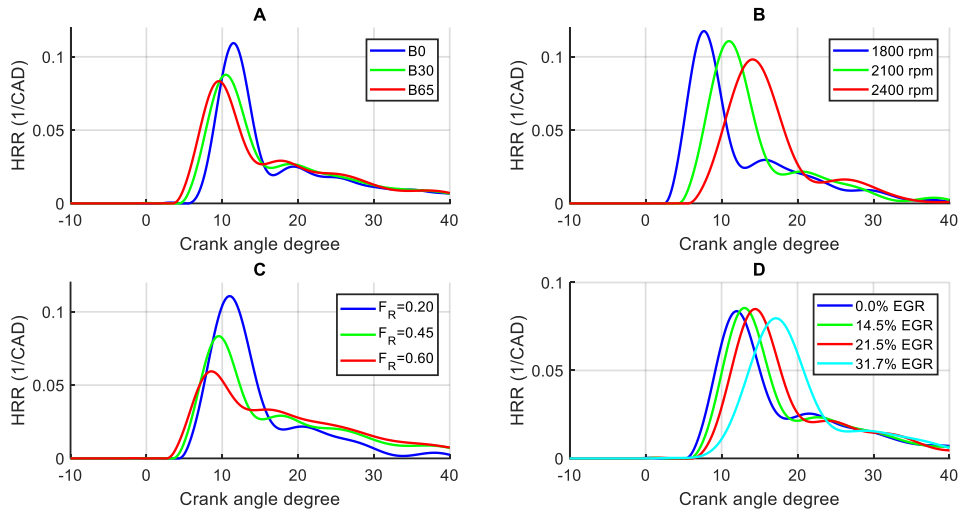

Fig. 12: Evolution of the normalized heat release rate (1/CAD). A: Different fuel mixtures at 2100 rpm, 0.45 fuel/air equivalence ratio, 0% external EGR. B: Different engine speeds for B65, 0.20 fuel/air equivalence ratio, 0% external EGR. C: Different fuel/air equivalence ratios for B65, 2100 rpm, 0% external EGR. D: Different percentages of external EGR for B65, 2400 rpm, 0.45 fuel/air equivalence ratio.

Fig. 12 (B) allows characterizing the influence of the engine speed on the HRR, concluding that the higher the speed, the lower are both the initial HRR gradient and its maximum value achieved. This behaviour is again related to the shorter time available for the evaporation and mixing of the fuel, as well as the cooling of the gases due to the progress of the expansion stroke.

Fig. 12 (C) presents the influence of the fuel/air equivalence ratio on the HRR. As mentioned at the beginning of this subsection, the absolute values of HRR (J / CAD) are not shown here, which would logically be higher the greater the fuel/air equivalence ratio considered. The main conclusion that derives from Fig. 12 (C) is associated with the fraction of heat released in each phase of combustion. In this way, the higher the fuel/air equivalence ratio, the more evident is the existence of a diffusive phase, despite the set of measures adopted to enhance the homogeneity of the mixture prior to the start of combustion. In other words, for low fuel/air ratios the predominant combustion is that corresponding to the premixed phase, with high levels of homogeneity according to the levels of NOx emissions, while for higher fuel/air ratios, on the contrary, the diffusive combustion acquires importance.

To conclude the analysis of the behaviour of the HRR, Fig. 12 (D) shows the influence of the percentage of external EGR. For values lower than 25%, it can be observed that, although a longer delay implies a lower temperature of the mixture, a higher percentage of external EGR implies a slight increase in the maximum value of HRR. Paradoxically, this is accompanied by a reduction in NOx emissions (Fig. 6), contrary to what occurs in conventional IC engines. Both the increase in the maximum HRR and the decrease in NOx emissions or the subsequent reduction in the combustion duration are attributable to the achievement of higher levels of homogeneity of the mixture, which are due to the greater time available associated with a longer ignition delay. For high values of external EGR, a decrease in the maximum value of the HRR is observed, which is attributable to the lower temperature of the mixture due to the progress of the expansion stroke, which leads to a lower reaction speed.

4.4. Analysis of combustion duration

The behaviour of the combustion duration will now be analysed. First, Fig. 13 represents the combustion angle versus the engine load, using different fuel mixtures as a parameter. The results show that the combustion duration is directly proportional to the load. This is due to the increased amount of fuel injected, which necessarily increases the time required to complete oxidation. Likewise, Fig. 13 reveals that, in global terms, the combustion of biodiesel has a slightly shorter duration, which can be attributed to the higher reaction speed derived from the higher average temperature of the gases associated with the shorter delay.

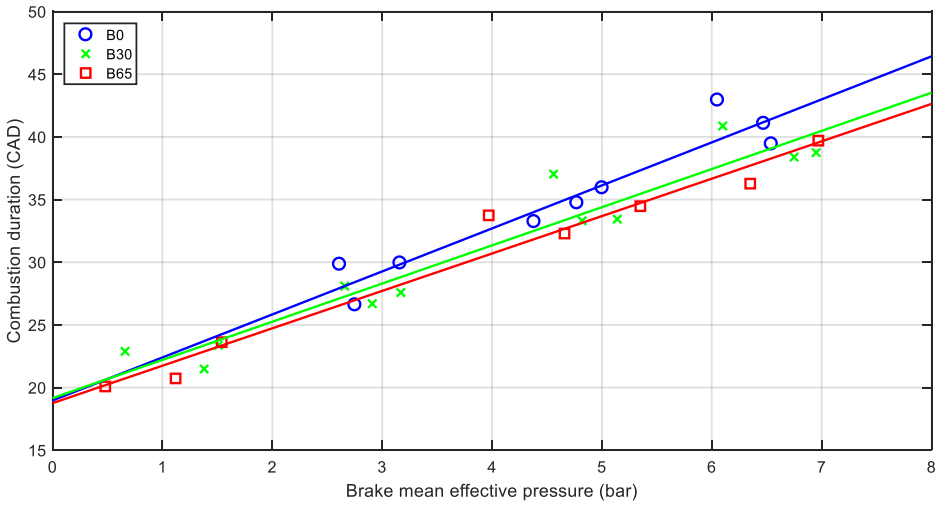

Fig. 13: Combustion duration (CAD) as a function of break mean effective pressure (bar), for different fuel mixtures at 0% external EGR, including 1800, 2100 and 2400 rpm.

Fig. 14 shows the decrease in combustion duration due to an increase in the percentage of external EGR. As mentioned previously, a higher percentage of EGR implies a longer ignition delay, which translates into a longer time available for homogenization of the mixture, which, finally, implies a faster combustion. This effect is striking, since the longer delays derived from an increase in external EGR lead to a lower average temperature of the gases, which reduces the combustion speed. Likewise, the aforementioned capacitive effect of the EGR also contributes to the decrease in the average temperature of the gases. Finally, the results shown in Fig. 14 (A and B) allow concluding that the dominant effect is that associated with the homogenization of the mixture, which results in a shorter combustion duration. To conclude the analysis of the combustion duration, Fig. 14 (B) allows characterizing the influence of the engine speed, concluding that the higher the speed, the longer the combustion duration. This behaviour is again attributable to the fact that the decrease in combustion time derived from the increase in turbulence caused by the higher piston speed is proportionally less than the increase in the rotational speed.

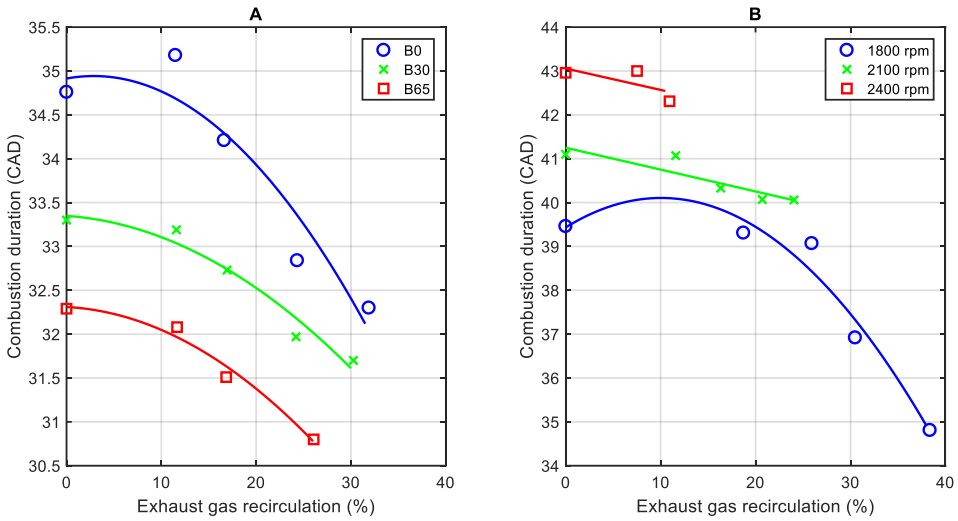

Fig. 14: Combustion duration (CAD) as a function of external EGR (%). A: Different fuel mixtures at 2100 rpm, 0.45 fuel/air equivalence ratio. B: Different engine speeds for B0, 0.60 fuel/air equivalence ratio.

4.5. Development of predictive correlations

To conclude the present study, the development of correlations that allow predicting both the ignition delay and the combustion duration based on different operating parameters is proposed. In the case of ignition delay, it should first be noted that the use of Arrhenius's law (Eq. 4) entails unacceptable levels of error [32].

$$\tau = A \cdot p^{-n} \cdot \exp\left(\frac{EA}{R \cdot T}\right) \qquad \text{Eq. 4}$$

For this reason, the use of polynomial correlations is proposed, which have allowed obtaining satisfactory results in similar applications [32] [33] [34]. The validity of such a predictive approach is limited to the operating conditions used for determining the model parameters, which are defined in Table 4. However, before fitting the correlation coefficients, a multifactorial variance analysis is performed in order to determine the factors that have a statistically significant effect on ignition delay. The results of this statistical analysis, which are summarized in Fig. 15, show that all of the four operating variables analysed (% biodiesel, speed, fuel/air equivalence ratio and % external EGR) are statistically significant in relation to delay:

$$\tau = f(\%bio, rpm, F, \%EGR) \qquad \text{Eq. 5}$$

On the other hand, the function that will be used to develop the delay correlation will be a cubic polynomial without interactions, thus limiting the potential appearance of the Runge phenomenon, consisting of significant numerical oscillations for points located outside the calibration range of the correlation produced by higher order terms [29]. This decision implies that the adjustment of 13 coefficients is necessary, which were determined by applying a least squares fitting procedure (Table 6). The goodness of the results obtained through this method is shown in Fig. 16 ($R^2 = 0.960$), highlighting that the maximum error made in the prediction of the ignition delay is less than 1.4 CAD, which is considered very good accuracy [29].

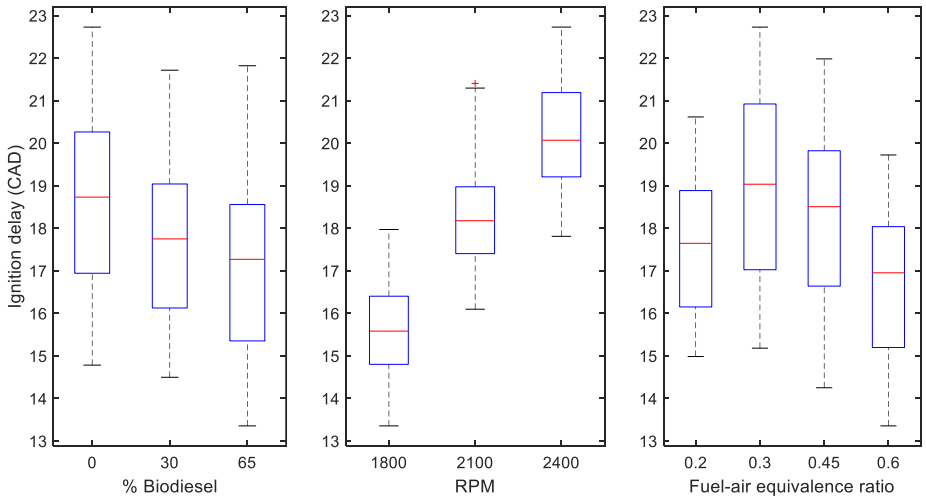

Fig. 15: Box plot of ignition delay (CAD) versus biodiesel percentage (%), speed (rpm) and fuel/air equivalence ratio (-).

Table 6: Correlation coefficients for predicting the ignition delay.

	%bio	rpm	F	%EGR
x^0		-20.27		
x^1	-4.20	294.57	14.00	-3.36
x^2	3.02	-618.77	-31.75	56.80
x^3	-0.18	323.21	14.63	-82.28

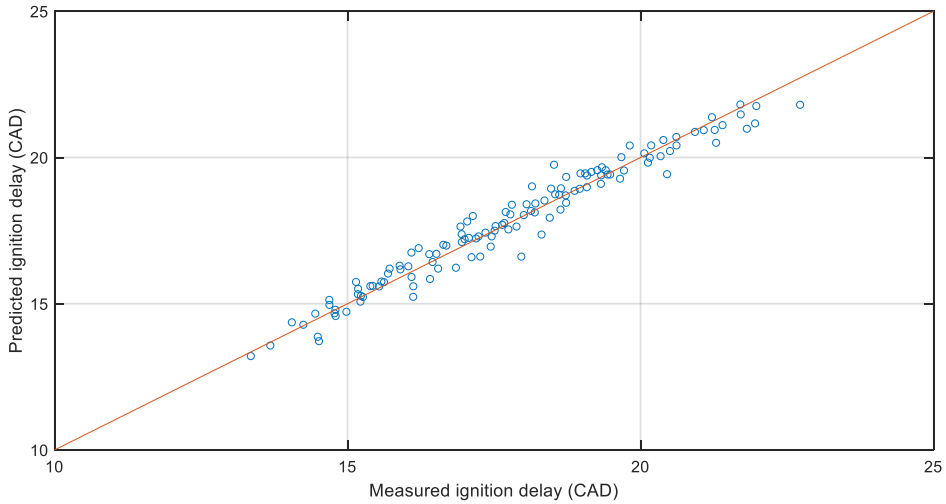

Fig. 16: Comparison between predicted and measured ignition delay (CAD). $R^2 = 0.960$.

The same procedure is applied to obtain the correlation corresponding to the combustion duration. However, in this case, in addition to the four operating parameters previously considered, the ignition delay will be added as a covariate:

$$\Delta\theta = f(\%bio, rpm, F, \%EGR, \tau) \qquad \text{Eq. 6}$$

A statistical study allows finding that the strongest dependence derives from the fuel/air equivalence ratio and, to a lesser extent, from the speed and the percentage of biodiesel (Fig. 17). The least squares adjustment of the 16 coefficients (Table 7) involved

in the cubic polynomial without interactions results in the predictions shown in Fig. 18, which again stand out for their accuracy ($R^2 = 0.971$).

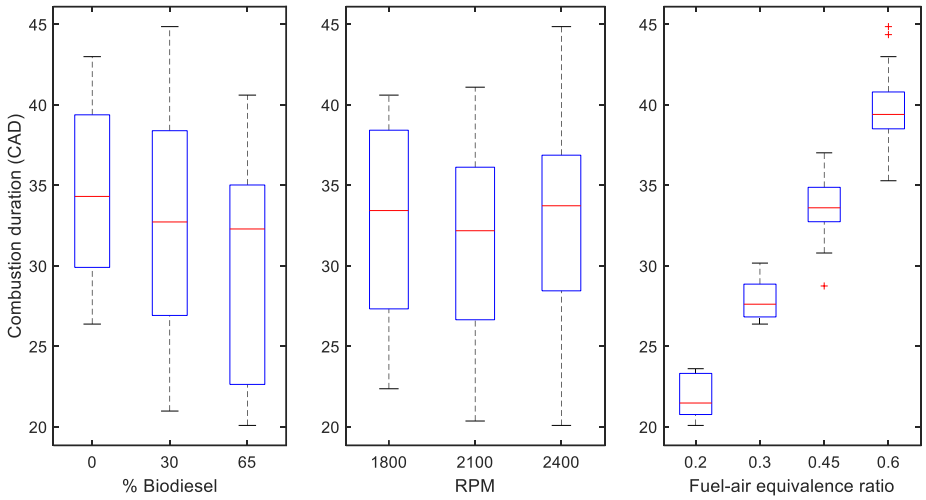

Fig. 17: Box plot of combustion duration (CAD) versus biodiesel percentage (%), speed (rpm) and fuel/air equivalence ratio (-)

Table 7: Correlation coefficients for predicting combustion duration.

	%bio	rpm	F	%EGR	τ
x^0			76.98		
x^1	859.04	-554.14	95.95	2.95	-229.39
x^2	-4060.51	1728.47	-116.87	22.78	237.58
x^3	4230.84	-470.22	67.87	-45.58	193.34

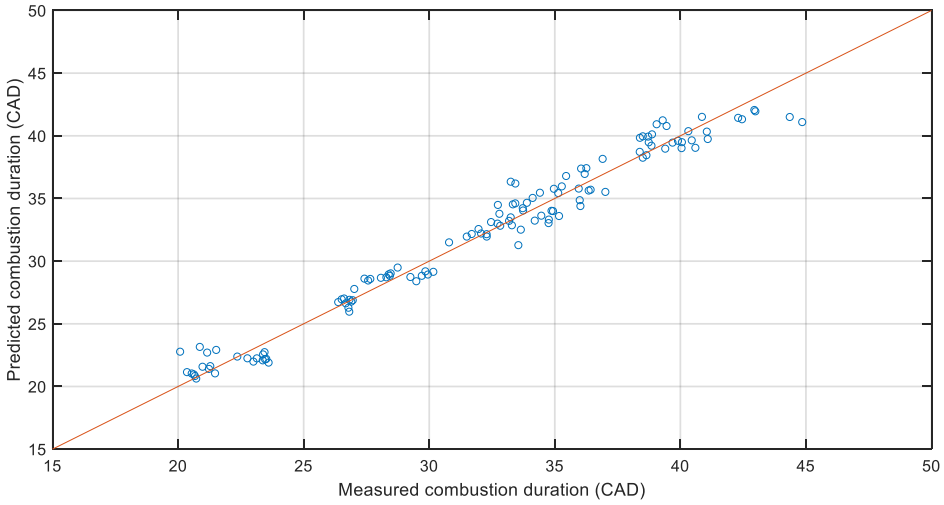

Fig. 18: Comparison between predicted and measured combustion duration (CAD). $R^2 = 0.971$.

5. Conclusions

The analysis performed has allowed deepening the knowledge of the combustion process of different biodiesel blends in a CI engine modified to operate with late direct injection. The results about pollutant emissions allow concluding that the measures adopted to enhance the homogeneity of the mixture have been satisfactory despite the

difficulties stemming from the higher viscosity and density of biodiesel. In particular, the success of the measures taken to reduce NOx emissions (< 50% compared to the original engine configuration), without entailing a reduction in engine performance (only a 6.9% shortfall in BMEP), has been demonstrated. It is worth highlighting the need to promote ignition delay as a necessary measure to decrease the temperature of the mixture and increase its degree of homogeneity, highlighting the effectiveness of the external EGR and the internal turbulence induction mechanisms.

The aforementioned aspects suggest that by modifying the configuration of the original engine, an advanced combustion mode has been achieved, intermediate between that used in conventional CI engines and HCCI combustion. This conclusion is mainly supported by the low levels of NOx emissions achieved. However, the HRR curves obtained show a diffusive stage, which is not present in typical combustion in HCCI mode. This fact suggests that the homogeneity achieved, although greater than in a conventional IC engine, is not complete.

Regarding the addition of different biodiesel fractions to the fuel used, it should be noted that the experimental results obtained show a significant reduction in soot emissions (55% for B65), as well as a higher brake efficiency (4% increase of maximum brake efficiency for B65), a shorter autoignition delay (2.0 CAD for B65) and a shorter combustion duration (2.5 CAD for B65). The mentioned reduction in soot emissions balances the well-known increase derived from the adoption of the late direct injection system.

The accuracy of the predictions derived from the correlations developed to model the delay ($R^2 = 0.960$) and the combustion duration ($R^2 = 0.971$) will facilitate carrying out new studies of this type, avoiding the need to carry out new experimental test campaigns or carry out intensive calculations like those associated with CFD codes. Finally, it should be noted that the authors are currently dedicating their research effort to the development of a predictive model for the combustion of biodiesel with late direct injection.

Acknowledgements

This work was supported by the Council for Economy, Knowledge, Business and University of the Regional Government of Andalusia, Spain (Ref. AT17-5934-US).

References

[1] Demirbas, A. Biodiesel from vegetable oils via transesterification in supercritical methanol, Energy Conversion and Management 43 (2002) 2349–2356.

[2] Lapuerta, M., Armas, O., & Rodriguez-Fernandez, J. Effect of biodiesel fuels on diesel engine emissions. Progress in Energy and Combustion Science 34(2) (2008) 198-223.

[3] Speidel, H. K., Lightner, R. L., & Ahmed, I. Biodegradability of new engineered fuels compared to conventional petroleum fuels and alternative fuels in current use, Applied Biochemistry and Biotechnology 84 (2000) 879–897.

[4] McCormick, R.L., Graboski, M.S., Alleman, T.L., Hearing, A.M., & Tyson, K.L. Impact of biodiesel source material and chemical structure on emissions of criteria pollutants from a heavy-duty engine, Environmental Science & Technology 35 (2001) 1742–1747.

[5] Krahl, J., Munack, A., Bahadir, M., Schumacher, L., & Elser, N. Review: Utilization of Rapeseed Oil, Rapeseed Oil Methyl Ester or Diesel Fuel: Exhaust gas emissions and estimation of environmental effects. SAE Special Publications 1208 (1996) 311-330.

[6] Mueller, C. J., Boehman, A. L., & Martin, G. C. An experimental investigation of the origin of increased NOx emissions when fueling a heavy-duty compression-ignition engine with soy biodiesel. SAE International Journal of Fuels and Lubricants 2(1) (2009) 789-816.

[7] Kirkpatrick, A. T. (2020). Internal Combustion Engines: Applied Thermosciences. John Wiley & Sons.

[8] Lee, T., & Reitz, R.D. The effect of intake boost pressure on MK (modulated kinetics) combustion, JSME International Journal 46 (2003) 451–459.

[9] Kimura, S., Aoki, O., Ogawa, H., Muranaka, S., & Enomoto, Y. New combustion concept for ultra-clean and high-efficiency small DI diesel engines (No. 1999-01-3681). SAE Technical Paper (1999).

[10] Kimura, S., Aoki, O., Kitahara, Y., & Aiyoshizawa, E. Ultra-clean combustion technology combining a low-temperature and premixed combustion concept for meeting future emission standards. SAE Transactions (2001) 239-246.

[11] Miller, J. A., & Bowman, C.T. Mechanism and modeling of nitrogen chemistry in combustion, Prog. Energ. Combust. Sci. 15 (1989) 287-338.

[12] Rakopoulos, D. C., Rakopoulos, C. D., Giakoumis, E. G., & Dimaratos, A. M. Characteristics of performance and emissions in high-speed direct injection diesel engine fueled with diethyl ether/diesel fuel blends. Energy 43(1) (2012) 214-224.

[13] Rakopoulos, C. D., Rakopoulos, D. C., Kosmadakis, G. M., & Papagiannakis, R. G. Experimental comparative assessment of butanol or ethanol diesel-fuel extenders impact on combustion features, cyclic irregularity, and regulated emissions balance in heavy-duty diesel engine. Energy 174 (2019) 1145-1157.

[14] Nishijima, Y., Asaumi, Y., & Aoyagi, Y. Premixed lean diesel combustion (PREDIC) using impingement spray system. SAE Transactions (2001) 1738-1746.

[15] Hashimoto, K., Ohta, H., Hirasawa, T., Arai, M., & Tamura, M. Evaluation of ignition quality of LPG with cetane number improver. SAE Transactions (2002) 1462-1466.

[16] Rakopoulos, C. D., Rakopoulos, D. C., Mavropoulos, G. C., & Kosmadakis, G. M. Investigating the EGR rate and temperature impact on diesel engine combustion and emissions under various injection timings and loads by comprehensive two-zone modeling. Energy 157 (2018) 990-1014.

[17] Liu, C., & Karim, G. A. A simulation of the combustion of hydrogen in HCCI engines using a 3D model with detailed chemical kinetics. International Journal of Hydrogen Energy 33(14) (2008) 3863-3875.

[18] Rakopoulos, D. C. Effects of exhaust gas recirculation under fueling rate or air/fuel ratio–controlled strategies on diesel engine performance and emissions by two-zone combustion modeling. Journal of Energy Engineering 147(1) (2021) 04020079.

[19] Heywood, J. B. (2018). Internal Combustion Engine Fundamentals. McGraw-Hill.

[20] Rakopoulos, C. D., Antonopoulos, K. A., & Rakopoulos, D. C. Experimental heat release analysis and emissions of a HSDI diesel engine fueled with ethanol–diesel fuel blends. Energy 32(10) (2007) 1791-1808.

[21] Ramos, J. I. (1989*).* Internal *Combustion Engine Modeling*. Hemisphere Publishing Corporation.

[22] McBride, B. J. (2002). NASA Glenn *Coefficients for Calculating Thermodynamic Properties of Individual Species*. National Aeronautics and Space Administration, John H. Glenn Research Center at Lewis Field.

[23] Woschni, G. (1967). A universally applicable equation for the instantaneous heat transfer coefficient in the internal combustion engine. SAE Technical paper (1967) No. 670931.

[24] Jiménez-Espadafor, F. J., Garcia, M. T., Herrero, J. A. C., & Villanueva, J. A. B. Effect of turbulence and external exhaust gas recirculation on HCCI combustion mode and exhaust emissions. Energy & Fuels 23(9) (2009) 4295-4303.

[25] Rakopoulos, D. C., Rakopoulos, C. D., Giakoumis, E. G., Komninos, N. P., Kosmadakis, G. M., & Papagiannakis, R. G. Comparative evaluation of ethanol, n-butanol, and diethyl ether effects as biofuel supplements on combustion characteristics, cyclic variations, and emissions balance in light-duty diesel engine. Journal of Energy Engineering 143(2) (2017) 04016044.

[26] Liu, J., & Dumitrescu, C. E. Methodology to separate the two burn stages of natural-gas lean premixed-combustion inside a diesel geometry. Energy Conversion and Management 195 (2019) 21-31.

[27] Hu, S., Wang, H., Yang, C., & Wang, Y. Burnt fraction sensitivity analysis and 0-D modelling of common rail diesel engine using Wiebe function. Applied Thermal Engineering 115 (2017) 170-177.

[28] Lü, X., Chen, W., Ji, L., & Huang, Z. The effects of external exhaust gas recirculation and Cetane number improver on the gasoline homogeneous charge compression ignition engines, Combust. Sci. Tech. 178 (2006) 1237-1249.

[29] Sun, Y., Wang, H., Yang, C., & Wang, Y. Development and validation of a marine sequential turbocharging diesel engine combustion model based on double Wiebe function and partial least squares method. Energy Conversion and Management 151 (2017) 481-495.

[30] García, M. T., Aguilar, F. J. J. E., & Lencero, T. S. Experimental study of the performances of a modified diesel engine operating in homogeneous charge compression ignition (HCCI) combustion mode versus the original diesel combustion mode. Energy 34(2) (2009) 159-171.

[31] Milovanovic, N., & Chen, R. A review of experimental and simulation studies on controlled auto-ignition combustion. SAE paper 2001-01-1890 (2001).

[32] Maroteaux, F., & Saad, C. Diesel engine combustion modeling for hardware in the loop applications: Effects of ignition delay time model. Energy 57 (2013) 641-652.

[33] Awad, S., Varuvel, E. G., Loubar, K., & Tazerout, M. Single zone combustion modeling of biodiesel from wastes in diesel engine. Fuel 106 (2013) 558-568.

[34] Liu, J., & Dumitrescu, C. E. Single and double Wiebe function combustion model for a heavy-duty diesel engine retrofitted to natural-gas spark-ignition. Applied energy 248 (2019) 95-103.